Available online at www.sciencedirect.com

ScienceDirect

Journal of Crystal Growth 304 (2007) 472–475

JOURNAL OF CRYSTAL GROWTH

www.elsevier.com/locate/jcrysgro

$InAs_{0.3}Sb_{0.7}$ films grown on (1 0 0) GaSb substrates with a buffer layer by liquid-phase epitaxy

Fubao Gao[a,*], NuoFu Chen[a,b], Lei Liu[a], X.W. Zhang[a], Jinliang Wu[a], Zhigang Yin[a]

[a] *Key Laboratory of Semiconductor Materials Science, Institute of Semiconductors, Chinese Academy of Sciences, P. O. Box 912, Beijing 100083, China*
[b] *National Laboratory of Microgravity, Institute of Mechanics, Chinese Academy of Sciences, Beijing 100080, China*

Received 9 January 2007; received in revised form 15 March 2007; accepted 20 March 2007
Communicated by P. Rudolph
Available online 24 March 2007

Abstract

The growth of $InAs_xSb_{1-x}$ films on (1 0 0) GaSb substrates by liquid-phase epitaxy (LPE) has been investigated and epitaxial $InAs_{0.3}Sb_{0.7}$ films with $InAs_{0.91}Sb_{0.09}$ buffer layers have been successfully obtained. The low X-ray rocking curve FHWM values of $InAs_{0.3}Sb_{0.7}$ layer shows the high quality of crystal-orientation structure. Hall measurements show that the highest electron mobility in the samples obtained is $2.9 \times 10^4\,cm^2\,V^{-1}\,s^{-1}$ and the carrier density is $2.78 \times 10^{16}\,cm^{-3}$ at room temperature (RT). The $InAs_{0.3}Sb_{0.7}$ films grown on (1 0 0) GaSb substrates exhibit excellent optical performance with a cut-off wavelength of 12 μm.
© 2007 Elsevier B.V. All rights reserved.

PACS: 68.55.Jk; 81.15.Lm; 81.05.Ea

Keywords: A1. Crystal structure; A3. Liquid-phase epitaxy; B2. Semiconducting III–V materials

1. Introduction

Recently, there has been interest in ternary III–V alloys for long-wavelength infrared detector applications as an substitute to HgCdTe, which suffers from instability problems [1,2]. As an alternative to HgCdTe, $InAs_xSb_{1-x}$ grown on GaSb is a promising material for the realization of low-cost room-temperature (RT) detectors operating in the 3–5 and 8–14 μm wavelength devices due to its advantage of high electron mobility, faster response rate and high stability. When the value of x is in the mid-range ($0.2<x<0.5$), the $InAs_xSb_{1-x}$ alloy exhibits a large, positive "optical bowing" effect due to the ordering in the alloy [3–6], making possible its application in long-wavelength infrared detection. The band gap of $InAs_xSb_{1-x}$ goes through a minimum of about 0.1 eV near $x = 0.35$ and it is estimated that the associated wavelength response can be extended up to 12.5 μm.

For the $InAs_xSb_{1-x}$ film growth, some III–V compound semiconductors can be used for substrates such as GaAs, GaSb, InAs, InSb and InP. Because of the 6.9% difference in the lattice parameters of InAs and InSb, the epitaxy growth of mid-range $InAs_xSb_{1-x}$ films have been limited to molecular beam epitaxy (MBE) [7–10] and metal organic chemical vapor deposition (MOCVD) [11–14]. As is much more accessible and economical than MBE and MOCVD, liquid-phase epitaxy (LPE) is often considered for the growth of $InAs_xSb_{1-x}$ films. High-quality growth of $InAs_xSb_{1-x}$ films by LPE is only obtained at either end of the composition range corresponding to values of $x<0.15$ and $x>0.89$ [15–18]. Very recently, Peng et al. [19] have reported the growth of $InAs_{0.3}Sb_{0.7}$ films on GaAs substrates by LPE. While unfortunately, the $InAs_{0.3}Sb_{0.7}$ films obtained were polycrystalline. Hitherto, no report about the epitaxial growth of mid-range $InAs_xSb_{1-x}$ films by LPE has been found.

*Corresponding author. Tel.: +86 10 82304469; fax: +86 10 82304588.
E-mail address: fbgao@semi.ac.cn (F. Gao).

0022-0248/$ - see front matter © 2007 Elsevier B.V. All rights reserved.
doi:10.1016/j.jcrysgro.2007.03.011

Among the substrates of III–V materials, the lattice mismatch of GaSb and InSb is smaller than others. However, the melt point of InSb is lower (525 °C). So, in this work, GaSb was selected for substrate to reduce the impact of lattice mismatch because of its less lattice mismatch and appropriate melting point.

2. Experimental procedure

$InAs_xSb_{1-x}$ films were grown by a conventional horizontal graphite sliding-boat system with an ambient of flowing Pd membrane-purified hydrogen at atmospheric pressure in a quartz reactor tube. The furnace can provide a temperature profile with a temperature plateau long enough to accommodate entirely the graphite slider and a temperature-controlling accuracy of ± 0.1 °C. The starting materials were 6N pure In, Sb, and undoped polycrystalline InAs. The substrates were $10 \times 8 \times 0.5\,mm^3$ well-polished (1 0 0) n-type GaSb wafers, which were rinsed successively with tetrachloromethane, acetone, ethanol and de-ionized water in ultrasonic baths, and then etched in a solution of $CH_3COOH:H_2O:HF = 20:9:1$ before loading into the graphite boat. The $InAs_xSb_{1-x}$ films were grown by step-cooling method. According to our previous work [19], the optimum conditions for $InAs_{0.3}Sb_{0.7}$ films were obtained. The composition of the source material was In:Sb:InAs = 47.6:50.4:2.0 at weight ratio. The growth temperature is 549 °C. To allow the source materials to get proper homogenization, they were heated to 700 °C for 3 h together. After the temperature was cooled down to 590 °C, the GaSb substrate was put into the boat. Subsequently, the temperature was cooled down to 549 °C and the source melt was pushed onto the surface of the substrate. Constant growth temperature helps the uniformity of the $InAs_xSb_{1-x}$ films in the growth direction. Finally, the substrate was slid out of the melt and then the quartz reactor tube with the graphite boat was drawn out of the furnace.

In this work, we report the epitaxial growth of $InAs_{0.3}Sb_{0.7}$ films with buffer layers of $InAs_{0.91}Sb_{0.09}$ lattice matched to GaSb substrates to avoid the substrate dissolution on (1 0 0) n-type GaSb substrate by LPE technique and the thicknesses of the $InAs_xSb_{1-x}$ films are about 50 μm.

Structural properties of the epitaxial layers were evaluated by X-ray diffraction (XRD), scanning electronic microscopy (SEM). Compositional analyses were characterized by energy dispersive X-ray analysis (EDAX). And optical properties were examined by Fourier transform infrared (FTIR). Electrical properties were examined by Hall measurements. For Hall measurements, as well as FTIR and rocking curve characterizations, the substrates with the buffer layers were removed by grinding in order to eliminate their effects.

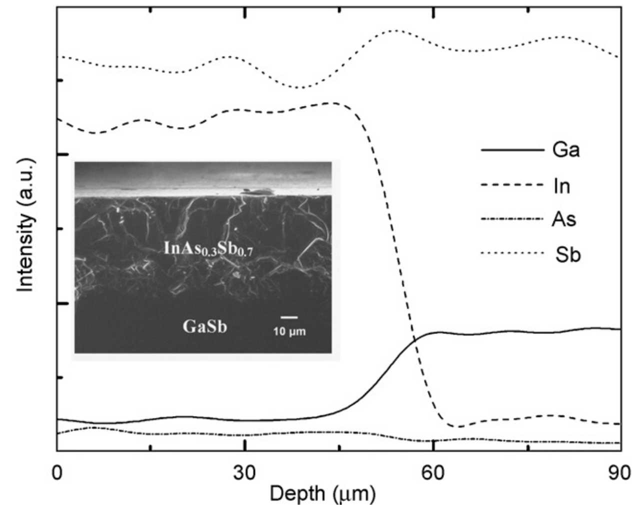

Fig. 1. Distribution of the constituent elements along the depth direction obtained from EDAX linescan for the $InAs_xSb_{1-x}$/GaSb film. Inset shows a cross section SEM image of the sample.

3. Results and discussion

Firstly, the $InAs_xSb_{1-x}$ films were grown directly on (1 0 0) n-type GaSb substrates by LPE. The inset of Fig. 1 shows a cross section image of the $InAs_xSb_{1-x}$/GaSb observed under SEM indicating a rough interface. By linescan of EDAX perpendicular to the surface in the cross section in Fig. 1, the distribution of the constituent elements along depth direction can be obtained. There has been elements interdiffusion in the interface and gallium was dissolved in the films. In general, attempts to grow $InAs_xSb_{1-x}$ films on GaSb from In-rich melts would result in rapid dissolution of the substrate because the thermodynamic tendency of the growth solutions is to dissolve GaSb substrates due to undersaturation with respect to antimony in the melt [15,16]. So, we adopted the scheme to grow a $InAs_{0.91}Sb_{0.09}$ buffer layer lattice matched to GaSb substrate. Because of the high melt point and stability of the $InAs_{0.91}Sb_{0.09}$ layer [15], the substrate dissolution could be avoided.

The cross section of the $InAs_xSb_{1-x}/InAs_{0.91}Sb_{0.09}$/GaSb epitaxial layer observed under a SEM clearly reflects the sharpness of the interface (the inset in Fig. 2). The EDAX linescan result of the sample is shown in Fig. 2, and interdiffusion at the interface did not occur. The As composition in the $InAs_xSb_{1-x}$ layer was $x = 0.3$, as determined by EDAX. Simultaneous elemental identification confirmed that the region scanned was indeed $InAs_{0.3}Sb_{0.7}/InAs_{0.91}Sb_{0.09}$/GaSb.

The composition of $InAs_xSb_{1-x}$ films from XRD is consistent with that obtained from EDAX. Fig. 3 shows a typical XRD pattern of the $InAs_{0.3}Sb_{0.7}/InAs_{0.91}Sb_{0.09}$/GaSb film. In Fig. 3, the strongest peak at 58.01° and a weak peak at 51.96° are attributed to the (0 0 4) reflection of the $InAs_{0.3}Sb_{0.7}$ film excited from K_α and K_β radiation of the Cu X-ray source, respectively. The $InAs_{0.3}Sb_{0.7}$ film

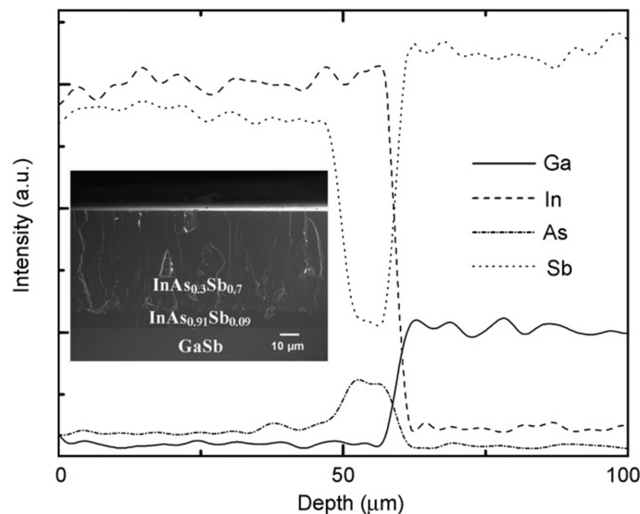

Fig. 2. Distribution of the constituent elements along the depth direction obtained from EDAX linescan for the $InAs_{0.3}Sb_{0.7}/InAs_{0.91}Sb_{0.09}/GaSb$ film. Inset shows a cross section SEM image of the sample.

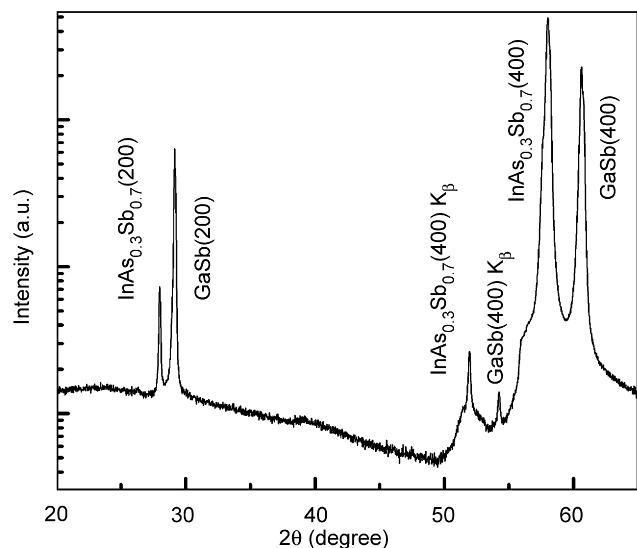

Fig. 3. X-ray diffraction pattern of the $InAs_{0.3}Sb_{0.7}/InAs_{0.91}Sb_{0.09}/GaSb$ film.

(0 0 2) peak can also be clearly observed. These results clearly indicate that the $InAs_{0.3}Sb_{0.7}$ film (0 0 1) planes are oriented parallel to the GaSb surface and the $InAs_{0.3}Sb_{0.7}$ film is a single crystal with (1 0 0) orientation. As seen in Fig. 4, the $InAs_{0.3}Sb_{0.7}$ film exhibits good quality values. Actually, the FWHM of the peak is smaller than the reported for epitaxial $InAs_xSb_{1-x}$ with similar composition grown by MBE [20].

The single-crystal structure of the $InAs_{0.3}Sb_{0.7}/InAs_{0.91}Sb_{0.09}/GaSb$ film has been confirmed as mentioned above. Then Hall measurements were performed on the sample with In contacts using the van der Paul method at 300 K. And the sample was fixed on a slide. The electron mobility of the $InAs_{0.3}Sb_{0.7}$ film grown on GaSb was as high as $2.9\times10^4 cm^2 V^{-1} s^{-1}$ with a carrier concentration

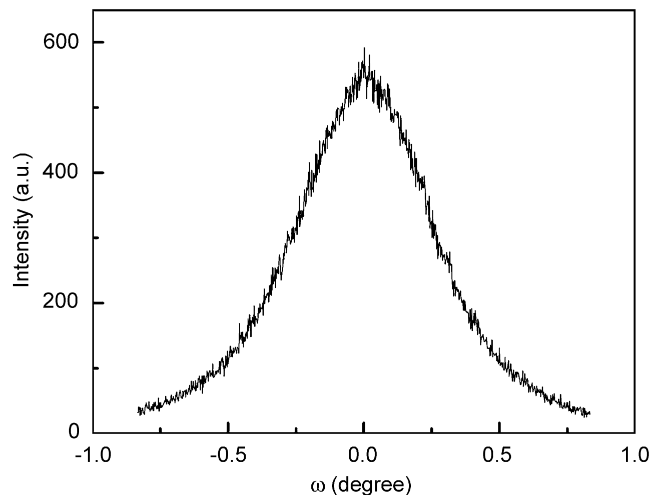

Fig. 4. The rocking curve of the $InAs_{0.3}Sb_{0.7}/InAs_{0.91}Sb_{0.09}/GaSb$ film.

(n-type) of $2.78\times10^{16} cm^{-3}$. These results are better than those reported for epitaxial $InAs_xSb_{1-x}$ films with similar composition grown by MOCVD [14] and MBE [8,21]. The electron mobility at RT is strongly affected by scattering of the crystal lattice. Thus, a high electron mobility at RT proved that the lattice perfection of the $InAs_{0.3}Sb_{0.7}$ epitaxial layer is quite good.

The FTIR transmission spectrum of the sample measured at RT is shown in Fig. 5. We defined the cutoff wavelength as the mid-transmittance wavelength and the absorption edges of the $InAs_{0.3}Sb_{0.7}$ film can be clearly observed in the spectrum. The cut-off wavelength of the $InAs_{0.3}Sb_{0.7}$ film is 12 μm at RT. This indicates that the absorption range of the $InAs_xSb_{1-x}$ film can cover the long wavelength transmission window in the atmosphere (8–14 μm), making its application in long-wavelength infrared detection possible. Since the cut-off wavelength of the $InAs_xSb_{1-x}$ film is much longer than that of InSb (about 7 μm at RT), a strong optical bowing effect has occurred to the $InAs_xSb_{1-x}$ film. According to Refs. [3–6], there is pronounced ordering in the $InAs_{0.3}Sb_{0.7}$ film.

Transmission spectrum recorded at RT show a shift in absorption edge towards the low-energy side for $InAs_{0.3}Sb_{0.7}$ in comparison to InSb. The inset in Fig. 5 shows that band tail is present in the transmission spectrum. A probable reason is the influence of the electric fields of charged defects [22]. Band tail may also be probably generated by agglomerate effect of positive ion and distortion potential of lattice and built-in electric field of deep-level center [23]. For a direct energy gap semiconductor, the absorption coefficient (α) of $InAs_xSb_{1-x}$ can be described as $\alpha = A(h\nu-E_g)^{1/2}$, to the experimental data on the absorption edge. Here, α is the absorption coefficient in cm^{-1}, ν is the incident photon frequency and A is a constant depending on the electron and hole effective masses and the optical transition matrix element. Therefore, based on the data of αd (d is the film thickness) calculated from FTIR transmission results, the

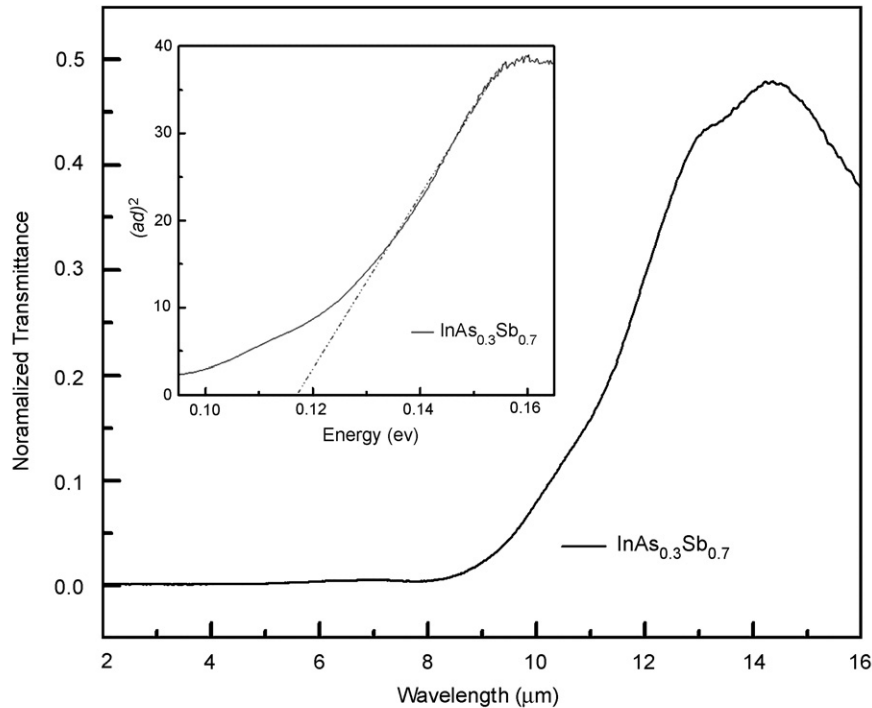

Fig. 5. FTIR spectra at RT of the $InAs_{0.3}Sb_{0.7}$ film. Inset shows the corresponding for linear fitting.

RT energy gap thus calculated was 0.117 eV for the $InAs_{0.3}Sb_{0.7}/InAs_{0.91}Sb_{0.09}/GaSb$ film. The dependence of E_g on the composition of $InAs_xSb_{1-x}$ at RT has been given by Woolley and Warner [24] as $E_g(x) = 0.35 - 0.771(1-x) + 0.596(1-x)^2$ (eV). This relation predicts $E_g(0.3) = 0.102$ eV at 300 K.

4. Conclusion

In conclusion, we have grown high-quality $InAs_xSb_{1-x}$ epitaxial layers on (1 0 0) GaSb substrates by LPE using step-cooling method. The microstructure of the epitaxial layers was analyzed using XRD, SEM and EDAX. The results obtained in this work allow the conclusion that the epitaxial layers have a good crystal quality. Furthermore, the $InAs_xSb_{1-x}$ films exhibit Hall mobility higher than $2.9 \times 10^4\,cm^2\,V^{-1}\,s^{-1}$. And a cut-off wavelength of 12 μm at RT obtained from FTIR, indicating that there is structural ordering in the $InAs_xSb_{1-x}$ films. Hence, LPE-grown $InAs_{0.3}Sb_{0.7}/InAs_{0.91}Sb_{0.09}/GaSb$ film has demonstrated attractive properties for use in RT long-wavelength infrared detectors. And since the growth cost of LPE is low, the application is economical yet.

Acknowledgments

This work was supported by Special Funds for Major State Basic Research Project 2002CB311905 and by the National Natural Science Foundation of China (Grant no. 60576010).

References

[1] T. Niedziela, R. Ciupa, Solid-State Electron. 45 (2001) 41.
[2] J.D. Kim, D. Wu, J. Wojkowski, J. Piotrowski, J. Xu, M. Razeghi, Appl. Phys. Lett. 68 (1996) 99.
[3] S.H. Wei, A. Zunger, Appl. Phys. Lett. 58 (1991) 2684.
[4] G.P. Srivastava, J.L. Martins, Alex Zunger, Phys. Rev. B 31 (1985) 2561.
[5] H.R. Jen, K.Y. Ma, G.B. Stringfellow, Appl. Phys. Lett. 54 (1989) 1154.
[6] S.R. Kurtz, L.R. Dawson, R.M. Biefeld, D.M. Follstaedt, B.L. Doyle, Phys. Rev. B 46 (1992) 1909.
[7] M.Y. Yen, B.F. Levine, C.G. Bethea, K.K. Choi, A.Y. Cho, Appl. Phys. Lett. 50 (1987) 927.
[8] M.Y. Yen, R. People, K.W. Wecht, J. Appl. Phys. 64 (1988) 952.
[9] J.-1. Chyi, S. Kalem, N. S. Kumar, C.W. Litton, H. Morkoc, 53 (1988) 1092.
[10] S. Tsukamoto, P. Bhattacharya, Y.C. Chen, J.H. Kim, J. Appl. Phys. 67 (1990) 6819.
[11] P.K. Chiang, S.M. Bedair, J. Electrochem. Soc. 131 (1984) 2422.
[12] P.K. Chiang, S.M. Bedair, Appl. Phys. Lett. 46 (1985) 383.
[13] R.M. Biefeld, C.R. Hills, S.R. Lee, J. Crystal Growth 91 (1988) 515.
[14] J.D. Kim, D. Wu, J. Wojkowski, J. Wojkowski, J. Xu, M. Razeghi, Appl. Phys. Lett. 68 (1996) 99.
[15] Y. Mao, A. Krier, J. Crystal Growth 133 (1993) 108.
[16] J.R. Skelton, J.R. Knight, Solid-State Electron. 28 (1985) 1166.
[17] J.L. Zyskind, A.K. Srivastrava, J. Appl. Phys. 61 (1987) 2898.
[18] V.K. Dixit, B. Bansal, V. Venkataraman, H.L. Bhat, K.S. Chandrasekharan, B.M. Arora, J. Appl. Phys. 96 (2004) 4989.
[19] C.T. Peng, N.F. Chen, F.B. Gao, X.W. Zhang, C.L. Chen, W.J. Liang, Y.D. Yu, Appl. Phys. Lett. 88 (2006) 2108.
[20] H. Miyoshi, Y. Horikoshi, J. Crystal Growth 227–228 (2001) 571.
[21] C.G. Bethea, M.Y. Yen, B.F. Levine, K.K. Choi, Appl. Phys. Lett. 51 (1987) 1431.
[22] D. Redfield, Phys. Rev. 130 (1963) 916.
[23] J.H. Chu, Band Gap Semiconductors Physics, Science Press, Beijing, 2005, p.199.
[24] J.C. Woolley, J. Warner, Can. J. Phys. 42 (1964) 1879.